

Robust ENSO across a Wide Range of Climates

GEORGY E. MANUCHARYAN AND ALEXEY V. FEDOROV

Department of Geology and Geophysics, Yale University, New Haven, Connecticut

(Manuscript received 10 December 2013, in final form 6 April 2014)

ABSTRACT

El Niño–Southern Oscillation (ENSO) is a pronounced mode of climate variability that originates in the tropical Pacific and affects weather patterns worldwide. Growing evidence suggests that despite extensive changes in tropical climate, ENSO was active over vast geological epochs stretching millions of years from the late Cretaceous to the Holocene. In particular, ENSO persisted during the Pliocene, when a dramatic reduction occurred in the mean east–west temperature gradient in the equatorial Pacific. The mechanisms for sustained ENSO in such climates are poorly understood. Here a comprehensive climate model is used to simulate ENSO for a broad range of tropical Pacific mean climates characterized by different climatological SST gradients. It is found that the simulated ENSO remains surprisingly robust: when the east–west gradient is reduced from 6° to 1°C, the amplitude of ENSO decreases only by 30%–40%, its dominant period remains close to 3–4 yr, and the spectral peak stays above red noise. To explain these results, the magnitude of ocean–atmosphere feedbacks that control the stability of the natural mode of ENSO (the Bjerknes stability index) is evaluated. It is found that as a result of reorganization of the atmospheric Walker circulation in response to changes in the mean surface temperature gradient, the growth/decay rates of the ENSO mode stay nearly constant throughout different climates. These results explain the persistence of ENSO in the past and, in particular, reconcile the seemingly contradictory findings of ENSO occurrence and the small mean east–west temperature gradient during the Pliocene.

1. Introduction

A salient feature of the present-day climate is the zonal asymmetry of sea surface temperatures (SST) in the tropical Pacific, characterized by a vast warm pool in the west and a strong cold tongue in the east. This east–west SST difference and the entire ocean thermal structure along the equator are tightly coupled to the easterly trade winds of the atmospheric zonal circulation (the Walker cell); interactions between these components of the tropical climate allow for a quasi-periodic oscillation, known as ENSO, in which the winds and the SST gradient relax (El Niño) and strengthen (La Niña) interannually (e.g., Philander 1990; Clarke 2008; Sarachik and Cane 2010).

How this oscillation changes when tropical climate changes is an important question for both present-day climate and paleoclimates (Fedorov and Philander 2000, 2001; Yeh et al. 2009; Collins et al. 2010; Cobb et al. 2013; Koutavas et al. 2006). Although climate models

currently predict relatively modest future changes in the mean SST gradient and ENSO, mainly because of compensation between different mechanisms controlling both the mean climate and its variability (DiNezio et al. 2009, 2012), the reliability of these projections is uncertain in view of large differences between the models (Collins et al. 2010; Guilyardi et al. 2009; Watanabe et al. 2012; Brown et al. 2011), which often disagree even on the sign of changes. Consequently, potential shifts in El Niño characteristics with rising atmospheric CO₂ concentration remain a matter of concern. To build confidence in climate projections, understanding past changes in the mean state of the tropics and ENSO is crucial.

Available observational evidence suggests that ENSO was active as far back as the late Cretaceous (Davies et al. 2012, 2011), Eocene (Huber and Caballero 2003; Ivany et al. 2011), Miocene (Galeotti et al. 2010), Pliocene (Scroton et al. 2011; Watanabe et al. 2011), and Pleistocene (Rittenour et al. 2000; Cane 2005) epochs (Fig. 1) and persisted with some changes through the Holocene (Cobb et al. 2013; Koutavas et al. 2006; Brown et al. 2006; Cobb et al. 2003; McGregor et al. 2013). While there are a large variety of coral data from

Corresponding author address: Georgy Manucharyan, 210 Whitney Ave., Kline Geology Laboratory, New Haven, CT 06511.
E-mail: georgy.manucharyan@yale.edu

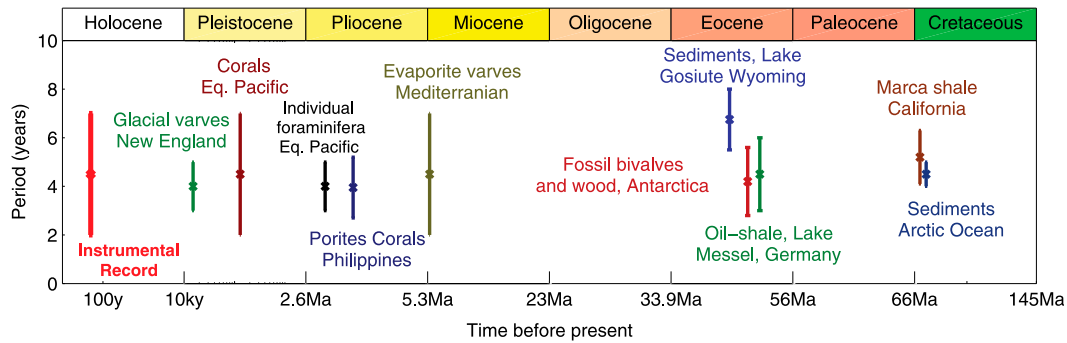


FIG. 1. Geological evidence suggesting ENSO-like variability in past climates. Vertical bars indicate the dominant frequency bands identified in geological samples from different epochs spanning from the late Cretaceous to the Pleistocene [data compiled from Davies et al. (2012, 2011), Huber and Caballero (2003), Ivany et al. (2011), Galeotti et al. (2010), Scroton et al. (2011), Watanabe et al. (2011), Rittenour et al. (2000), and Cane (2005)]. For a review of the Holocene data see Cane (2005). The date bands are given as reported in the original studies and should be interpreted with caution, since different methods have been used to estimate the range of dominant variability. Also, most of this geological evidence is based on the assumption of the same teleconnections as observed in the present-day climate and as such provide only tentative evidence for ENSO.

the Holocene providing proxy observations of ENSO from sites located within the equatorial Pacific, geological evidence is much more limited and uncertain for earlier time epochs. For example, the varved records from Mediterranean, England, and Antarctica, found to bear a signature of interannual variability, provide only a hypothetical link to ENSO-like climate variability through assumed teleconnections to the tropics.

The early Pliocene climate, having atmospheric CO_2 concentration between 350 and 400 ppm, draws particular attention as a potential analog for modern greenhouse conditions (Fedorov et al. 2013). Proxy records (Fedorov et al. 2013; Wara et al. 2005; Fedorov et al. 2006; Dekens et al. 2008) indicate that during that time the mean east–west SST gradient was small, perhaps on the order of or below $1^\circ\text{--}2^\circ\text{C}$, which is sometimes referred to as “permanent El Niño–like” conditions or “El Padre” (Ravelo 2008). Apparently, the warm pool SST stayed fairly constant, whereas the cold tongue surface and subsurface temperatures (Ford et al. 2012) were significantly warmer. Nevertheless, recent studies have discovered tentative evidence of a persistent ENSO activity during the Pliocene (Scroton et al. 2011; Watanabe et al. 2011). Even though some geological evidence should be treated with caution, these findings raise an important question of whether the permanent El Niño–like conditions can still sustain interannual variability. Even more generally, how do changes in the mean east–west SST gradient and related characteristics of the tropical mean state (e.g., mean winds, thermocline depth, and ocean stratification) affect ENSO properties?

So far, the connection between ENSO and the mean tropical climate has been explored in a broad parameter range within simple, intermediate, and hybrid models

(e.g., Fedorov and Philander 2001; Wittenberg 2002; An and Jin 2000; Sun 2003; Sun et al. 2004), but not comprehensive coupled models, where the zonal temperature gradient is difficult to control. At the same time, intercomparisons of coupled models typically do not give consistent results on the connection between the mean state and ENSO (e.g., Bellenger et al. 2013; Brown et al. 2011; Guilyardi et al. 2009). In the present work we have devised an efficient way to alter the mean temperature in the eastern equatorial Pacific (between 6° and 1°C), while keeping temperature in the west nearly constant (Figs. 2 and 3a), within a state-of-the-art climate model. Our approach invokes the fact that the equatorial cold tongue is maintained by the upwelling of waters that travel toward the equator from the extratropics within the ocean shallow subtropical cells (STCs) (e.g., McCreary and Lu 1994; Gu and Philander 1997). Changing the temperature of those waters changes the cold tongue temperature.

To make use of this effect, we conduct numerical experiments in which we systematically modify upper-ocean vertical mixing in the extratropics. Increasing the mixing warms the waters subducted in the STC and eventually raises the temperature of the cold tongue (Fig. 2). In turn, tropical ocean–atmosphere interactions act to establish a new mean state in which weaker east–west SST gradient ΔT and zonal winds balance each other in the equatorial band (Fig. 3). Since perturbations are imposed far away from the equator, in the extratropics, they do not affect ENSO dynamics directly, but only through changes in this mean state in the tropics.

Recent modeling studies show that ocean mixing in the subtropics, induced for example by tropical cyclones, can indeed warm the equatorial cold tongue (Fedorov

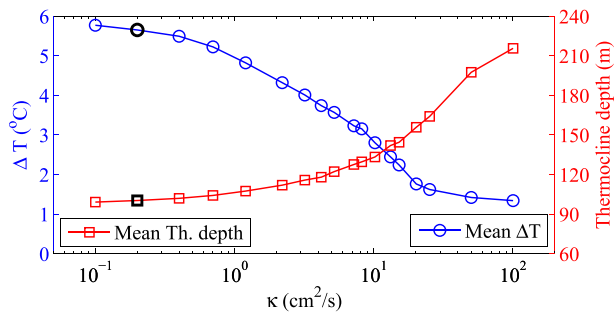


FIG. 2. The east–west SST gradient ΔT (blue) and zonally averaged thermocline depth (red) as a function of background diffusivity κ_b in the extratropical bands. Control run is denoted with black markers. The mean east–west temperature gradient is estimated as the difference between the maximum and minimum SST along the equator in the Pacific, averaged for the last 100 years of the computations. (Full SST and thermocline depth along the equator for each experiment are shown in Fig. 3.) The thermocline depth is defined here as the depth of the appropriate isotherm in each experiment (warmer isotherms are used for climates with smaller T) and hence reflects the upper-ocean heat content.

et al. 2010; Manucharyan et al. 2011). However, in the present study, we are not concerned with particular mechanisms that could alter ocean mixing. Rather, we simply use the extratropical mixing as an efficient tool to control tropical background conditions in a coupled climate model. While idealized, this approach allows us to explore a broad range of changes in the mean tropical climate.

2. Coupled climate model and experimental setup

The climate model used here is a version of the National Center for Atmospheric Research (NCAR) Community Earth System Model (CESM) that incorporates atmospheric and land surface models with a spectral truncation of T31 for the horizontal resolution [the Community Atmosphere Model, version 4 (CAM4), and the Community Land Model (CLM)] coupled to ocean and sea ice components [the Parallel Ocean Program, version 2 (POP2), and the Los Alamos sea ice model (CICE)] with a nominal 3° resolution increasing to 1° near the equator (Shields et al. 2012). This version of CESM with a medium resolution greatly facilitates sensitivity and paleoclimate simulations (the model source code and boundary conditions, are accessible online at <http://www.cesm.ucar.edu/models/cesm1.0/>). The integrations start from a preexisting preindustrial simulation and last for 300–600 years, depending on the experiment. This time is sufficient for the upper ocean to reach statistical equilibrium with the deep ocean experiencing a weak residual drift (Manucharyan et al. 2011). The analysis of the model output including SST and winds

stress is performed on fields averaged between 2.5°S and 2.5°N , with the Niño-3 region defined as 2.5°S – 2.5°N , 90° – 150°W . Note that here, in order to capture only regions with high SST variance, we have defined the Niño-3 region with latitudinal extent of 2.5°S – 2.5°N instead of conventional 5°S – 5°N .

Throughout the numerical experiments, we vary background vertical diffusivity in the extratropical bands (15° – 40° latitude and 0–400 m) within the range from -0.1 to $100 \text{ cm}^2 \text{ s}^{-1}$. The other spatially and time varying components of vertical diffusivity, computed by the model itself, are not explicitly modified in these experiments. In one experiment, to reduce the mixing, we multiplied the model original background diffusivity by 0.1, also in the extratropical bands. In addition, to check the robustness of our results, we perform two high-resolution simulations (with the ocean nominal latitudinal resolution close to 1° but decreasing to $\sim 1/4^{\circ}$ toward the equator), including a preindustrial control and a simulation with a large diffusivity ($\kappa_v = 50 \text{ cm}^2 \text{ s}^{-1}$).

In general, the effect of mixing increases with higher diffusion and with the greater depth of the mixing bands. For our study, these bands are chosen sufficiently far away from the equator, much farther than the typical baroclinic Rossby radius of deformation for the equatorial ocean ($\sim 4^{\circ}$). Therefore, the imposed perturbations in ocean vertical mixing do not affect ENSO dynamics directly, but only through changes in the background state of the tropics.

3. Simulated mean tropical climates and ENSO

As we alter the extratropical mixing, we are able to simulate a broad range of tropical Pacific climates that are dramatically different from its present-day conditions (Fig. 2). Throughout our experiments, the mean zonal SST gradient along the equator ranges from 6° to 1.3°C (5.6°C in the control run), while the maximum warm pool temperature stays nearly constant (Figs. 2 and 3a). The mechanism of the warming of the cold tongue due to enhanced ocean mixing can be understood from a heat budget perspective—a stronger mixing in the extratropics induces anomalous ocean heat gain over this region, weakening oceanic heat transport from the equatorial region and increasing the cold tongue temperature (Fedorov et al. 2010; Manucharyan et al. 2011). Reducing the mixing has an opposite effect.

Associated with a reduced SST gradient and the eastward expansion of the warm pool are the weakening of the atmospheric Walker circulation manifested in reduced trade winds and the broadening of the convection region. Furthermore, we observe the reduction in the upwelling consistent with the reduced trade winds and

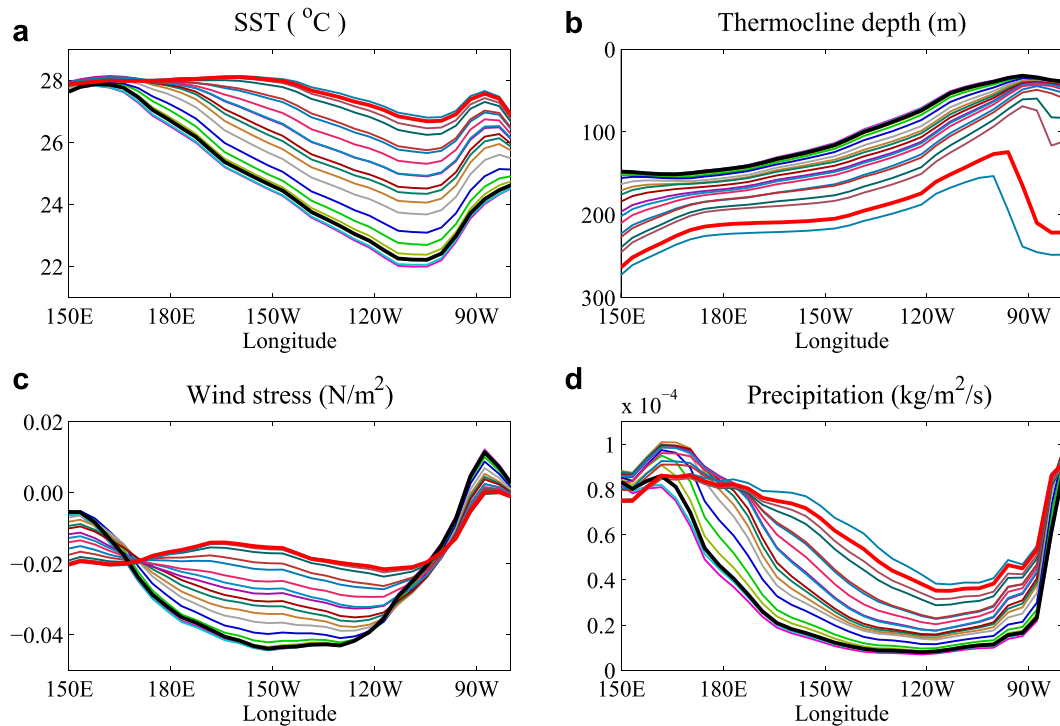


FIG. 3. Mean tropical climate in different experiments. Profiles of (a) mean SST, (b) thermocline depth, (c) wind stress, and (d) precipitation in the equatorial Pacific for numerical experiments with different values of ocean diffusivity in the extratropics. Note the large changes in the cold tongue temperature (in the east) but little change in the warm pool (in the west). Black and red lines, respectively, indicate present-day and a reduced-gradient climates ($\Delta T = 5.6^\circ$ and 1.4°C). For smaller values of ΔT note the shift of the maximum wind stress from the central to eastern Pacific and an increase in precipitation over the central and eastern Pacific, which reflect the corresponding shift in atmospheric convection.

the deepening of the thermocline (Figs. 2 and 3) reflecting the upper-ocean heat content increase.

Note that Fedorov and Philander (2000, 2001) investigated how independent changes in the mean wind, thermocline depth, and so on affected ENSO. While this was possible within the idealized setting of their intermediate coupled model, in a comprehensive climate model used in the present study all of these characteristics are tightly coupled. Nevertheless, we denote different tropical climates by their value of ΔT since it is a major feature of both atmospheric and oceanic dynamics. It is important to note, however, that ENSO dynamics in the model depends not only on ΔT but on the entire background climate state, including thermocline depth, mean winds, and other factors.

Across all the experiments, ENSO remains the most prominent part of the climate signal with the Niño-3 index (Fig. 4) capturing the zone of the highest SST variance in the eastern equatorial Pacific. The standard deviation of this index in the model reaches 0.9°C for the present-day climate but reduces to $0.5^\circ\text{--}0.7^\circ\text{C}$ for smaller ΔT (Fig. 5a), although the magnitude of strong events

decreases more noticeably. The power spectra of the Niño-3 index display statistically significant peaks in the interannual frequency range in all experiments (Fig. 6). The dominant period increases slightly for smaller ΔT (Fig. 5b); however, this increase should be considered in the context of the broad width of the spectral peaks. Note that ENSO is also prominently present in the high-resolution simulations of a reduced gradient climate ($\Delta T = 2^\circ\text{C}$), with variance and periods in rough agreement with medium-resolution runs (Fig. 5).

The main features of ENSO, such as the eastward propagation of thermocline depth anomalies or the coupling of wind anomalies to SSTs, are all present in our experiments (Fig. 7). The dynamics are governed by the recharge–discharge mechanism (e.g., Jin 1997a,b; Meinen and McPhaden 2000) in which positive anomalies in the western Pacific ocean heat content (OHC) along the equator precede El Niño events by about a quarter of a period, with the lag ranging from 6 months in our control run to nearly 10 months in the reduced ΔT climates (Fig. 8). These OHC anomalies, usually referred to as ocean heat recharge, occur as a result of

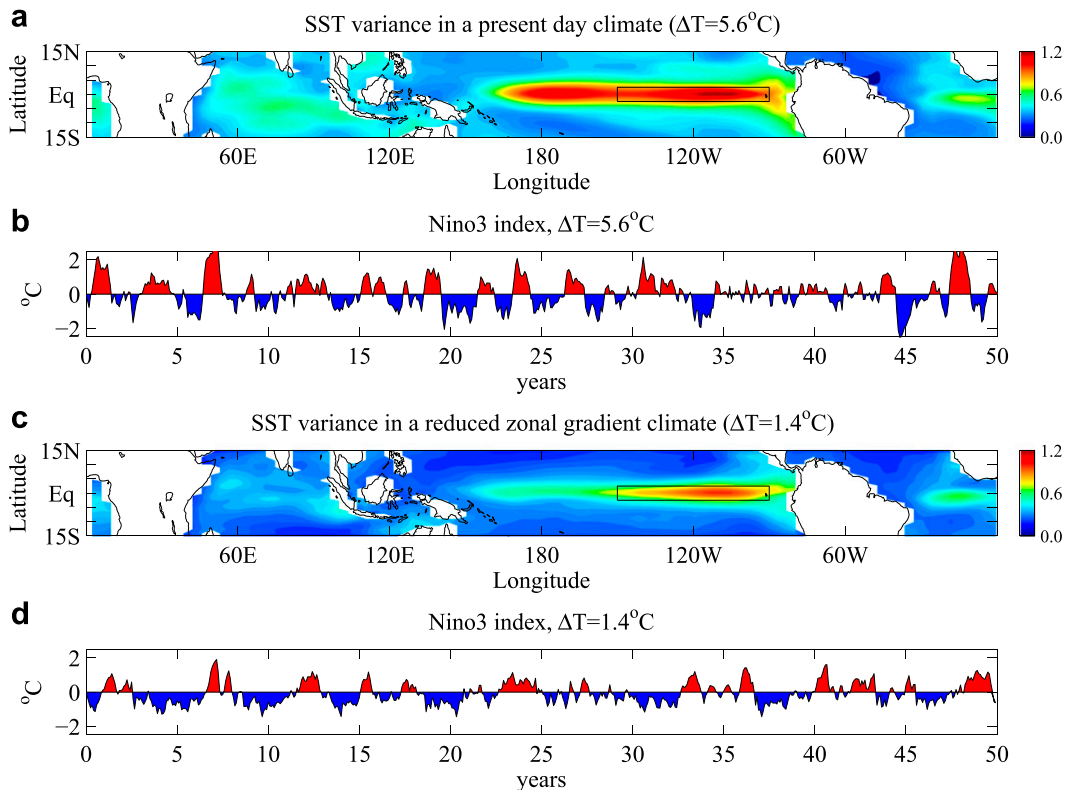


FIG. 4. SST variability in the tropics for the simulated present-day climate ($\Delta T = 5.6^{\circ}\text{C}$) and a climate with a reduced SST gradient ($\Delta T = 1.4^{\circ}\text{C}$). (a),(c) SST variance ($^{\circ}\text{C}$, shaded) as a function of latitude and longitude. (b),(d) The corresponding time series of Niño-3 index indicating active ENSO in these two very different climate states.

meridional heat redistribution prior to an El Niño and provide an essential mechanism for the transition between warm and cold phases of ENSO. The recharge-oscillator mechanism is closely related to the delayed oscillator and other simple models of ENSO (e.g., Fedorov 2010).

What explains this robustness of ENSO and relatively small changes in its properties across such dramatic changes in the mean equatorial climate? To answer this question, next we will evaluate the stability of the internal climate mode governing ENSO dynamics using a linearized heat budget equation for the Niño-3 region together with the recharge-oscillator approximations for ocean adjustment.

4. ENSO stability

The stability of the mode governing ENSO dynamics in the experiments is assessed by estimating the strengths of the relevant positive and negative feedbacks within the recharge-oscillator framework, following Jin et al. (2006). Here we extend their analysis to include an expression for the frequency of oscillations and, in particular, emphasize

the importance of the external noise in sustaining interannual variability.

a. The Bjerknes stability index

The Bjerknes stability index (Jin et al. 2006) is introduced using a linearized heat budget equation for a box encompassing the Niño-3 region in the upper ocean:

$$\frac{d}{dt}\langle T \rangle = 2I_{\text{BJ}}\langle T \rangle + F[h] \quad \text{and} \quad (1)$$

$$\frac{d}{dt}[h] = -c\langle T \rangle, \quad (2)$$

where T is surface temperature; h is the depth of the equatorial thermocline; the operators $\langle \cdot \rangle$ and $[\cdot]$ denote averages in the equatorial Pacific over the Niño-3 box and a zonal mean, respectively; I_{BJ} is the Bjerknes stability (BJ) index; and $F[h]$ represents the effect of the delayed ocean adjustment or ocean memory (Jin 1997a). Dynamical variables $\langle T \rangle$ and $[h]$ are perturbations from the climatological mean, whereas the time-independent coefficients are functions of the mean state of the equatorial Pacific.

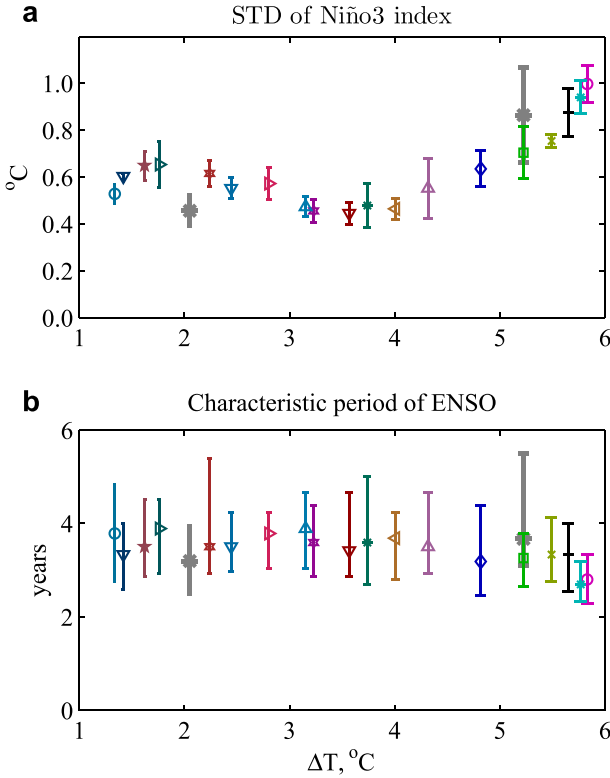


FIG. 5. The simulated amplitude and period of ENSO. (a) ENSO amplitude, defined as the standard deviation of the Niño-3 index. The error bars show its variation range between 25-yr intervals. (b) ENSO characteristic period, defined as the period corresponding to the maximum of the power spectrum in each experiment (see Fig. 6). The error bars give uncertainty based on the partial width of these peaks. Both the amplitude and the period are plotted as a function of the mean east–west SST gradient ΔT . The simulated present-day climate (control run) corresponds to $\Delta T = 5.6^{\circ}\text{C}$. Results from the two high-resolution simulations for $\Delta T = 5.2^{\circ}$ and 2°C are shown in thick gray.

Equation (2) describes variations in the mean thermocline depth and can be derived, for example, in the low-frequency approximation for the equatorial dynamics (Fedorov 2010). In principle, an additional damping term proportional to $[h]$ could be added to this equation to describe oceanic damping, but typically this term is small and is expected to remain fairly constant with climate change. As such, this term is neglected [also to be consistent with Jin et al. (2006)]. Also following Jin et al. (2006), to avoid complications when defining thermocline depth across different ocean states, we replace h with subsurface temperature at an 80-m depth. Changes in this temperature closely follow changes in the thermocline depth in the eastern Pacific.

The BJ index and the parameter F are composed of several contributions:

$$2I_{\text{BJ}} = -\left\langle \frac{\bar{u}}{L_x} \right\rangle - \left\langle \mathcal{H}(\bar{w}) \frac{\bar{w}}{H_m} \right\rangle - \alpha + \mu_a \beta_u \left\langle \frac{d\bar{T}}{dx} \right\rangle + \mu_a \beta_w \left\langle \mathcal{H}(\bar{w}) \frac{d\bar{T}}{dz} \right\rangle + \mu_a^* \beta_h \left\langle \mathcal{H}(\bar{w}) \frac{\bar{w}}{H_m} \right\rangle \quad \text{and} \quad (3)$$

$$F = -\beta_{uh} \left\langle \frac{d\bar{T}}{dx} \right\rangle + \left\langle \mathcal{H}(\bar{w}) \frac{\bar{w}}{H_m} \right\rangle. \quad (4)$$

Here, the overbar denotes the climatological mean quantities, $\mathcal{H}(w)$ is the Heaviside step function, x and z are the horizontal and vertical coordinates, and u and w are the zonal and vertical velocities. The horizontal and vertical extents of the averaging box are $L_x = 60^{\circ}$ longitude, $L_y = 5^{\circ}$ latitude, and $H_m = 80$ m, respectively; we have explored alternative definitions of the Niño-3 box and found some quantitative changes in magnitudes of different feedbacks, which however do not affect the main conclusions of the paper.

Combining Eqs. (1) and (2) we obtain a damped oscillator equation

$$\frac{d^2}{dt^2} \langle T \rangle - 2I_{\text{BJ}} \frac{d}{dt} \langle T \rangle + \Omega_0^2 \langle T \rangle = 0, \quad (5)$$

with the frequency $\Omega_0 = \sqrt{cF}$. The BJ index acts as a stability index for the oscillations governed by the recharge-oscillator model and gives the net growth (when positive) or decay rates (when negative) for the ENSO mode. In the latter case, external noise (or other forcing) is necessary to sustain continuous oscillations. These net growth or decay rates depend on key feedbacks that contribute to the mode stability, both negative and positive, all of which change in different climates.

b. Ocean–atmosphere coupling and linear feedbacks

The first three terms in Eq. (3) for the BJ index describe negative feedbacks—the mean zonal advection, upwelling, and surface heat flux feedbacks—while the last three terms represent the positive thermocline, Ekman pumping, and zonal advection feedbacks.

Negative advection feedbacks are associated with the mean flow (zonal and vertical) acting to damp Niño-3 temperature anomalies. The thermodynamic feedback (proportional to α) is associated with the surface heat fluxes, shortwave, longwave, latent, and sensible, which collectively act as a damping term. Its magnitude is computed as a linear regression of the net anomalous surface heat flux over the Niño-3 region onto the Niño-3 SST index.

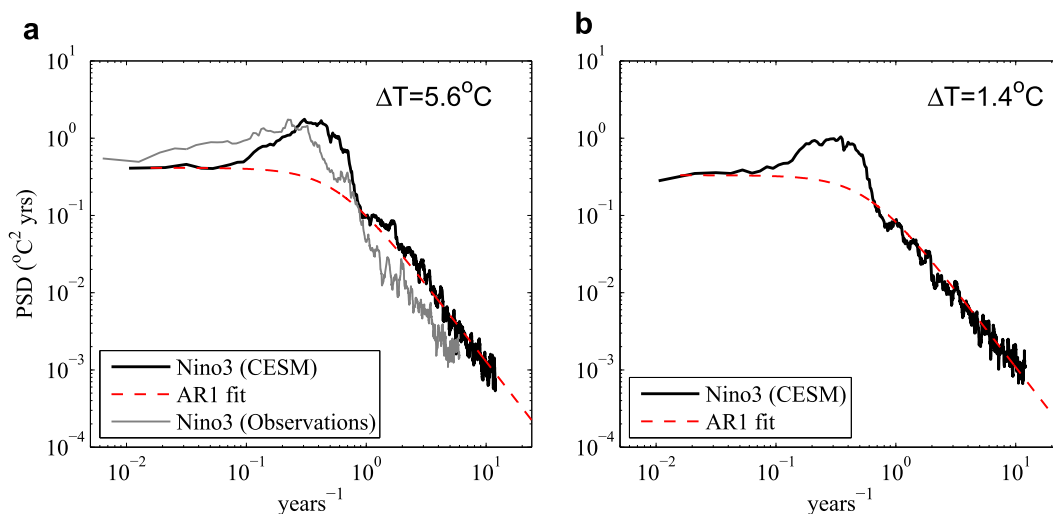


FIG. 6. Power spectra of the Niño-3 indices displayed in Fig. 4, for $\Delta T =$ (a) 5.6°C and (b) 1.4°C . The corresponding spectra for a first-order autoregressive (AR1) process (dashed red lines) and the observations (gray) are also shown. Note that interannual variability is clearly distinct from red noise in both climates.

The magnitudes of the positive advection, thermocline, and Ekman feedbacks in Eq. (3) depend on several sensitivity parameters [defined in Eqs. (5)–(8) of Jin et al. (2006)] that characterize ocean response to wind stress and atmospheric response to SST. For instance, the atmospheric sensitivity parameters μ_a and μ_a^* assume a linear response of Niño-3- and zonally averaged wind stress anomalies, respectively, to Niño-3 temperature anomalies. Analogously, the oceanic sensitivity parameters β_u and β_w assume a linear response of anomalous zonal and vertical velocities in the equatorial band to Niño-3 wind stress anomalies. Parameter β_h gives the linear sensitivity of the thermocline tilt (defined as $[h] - \langle h \rangle$) to the zonally averaged wind stress anomalies $[\tau]$. Particular values of these parameters are obtained by using linear regressions between the corresponding variables (Fig. 9). Before the computations, all the time series are smoothed to filter out short-scale variability.

One of the main factors destabilizing tropical climate is the thermocline feedback, in which SST in the eastern equatorial Pacific is modified by the mean upwelling of subsurface temperature anomalies associated with thermocline depth anomalies (induced by wind stress variations). This factor becomes a positive feedback via the coupling of wind stress to SST anomalies. When the cold tongue gets anomalously warm, the equatorial easterly winds relax, deepening the thermocline in the east and leading to further warming. As we move to climates with smaller ΔT , the effect of this feedback on the system increases at first but then substantially decreases (Fig. 10a).

These changes in the strength of the thermocline feedback result from several competing factors: weaker mean equatorial upwelling due to weaker zonal winds (Fig. 3c), a deeper ocean thermocline (Fig. 3b), and the reduced sensitivity of subsurface temperature (and thermocline tilt) to zonally averaged wind stress anomalies (Fig. 9c). In contrast, the ocean–atmosphere coupling, estimated through a linear regression of wind stress anomalies onto the Niño-3 index, increases (Fig. 9b) as the atmospheric Walker circulation becomes more sensitive to SST perturbations in warmer climates.

As the thermocline feedback weakens, it is the Ekman pumping feedback that becomes more destabilizing for smaller ΔT (Fig. 10a). In the Ekman feedback, SST is modified by anomalous upwelling acting on the mean thermal stratification. During warm episodes for example, a relaxation of zonal winds reduces upwelling of colder waters, facilitating the growth of initial SST perturbations. In the present-day climate, wind stress anomalies are most pronounced in the western equatorial Pacific (Fig. 11a), where the mean thermal stratification is weak, limiting the magnitude of the Ekman feedback. The wind stress pattern in Fig. 11a generally agrees with the analysis of observational datasets (e.g., Wittenberg 2004). However, for smaller ΔT , the region of atmospheric convection spreads eastward and wind stress anomalies move closer to SST anomalies in the eastern Pacific (Fig. 11b), which amplifies the Ekman feedback (Fig. 10a) owing to the strong increase in the local coupling coefficient μ_a (Fig. 9a). A similar mechanism works to strengthen the zonal advection feedback, but the latter remains relatively weak. Overall, positive feedbacks intensify for smaller ΔT (Fig. 10c).

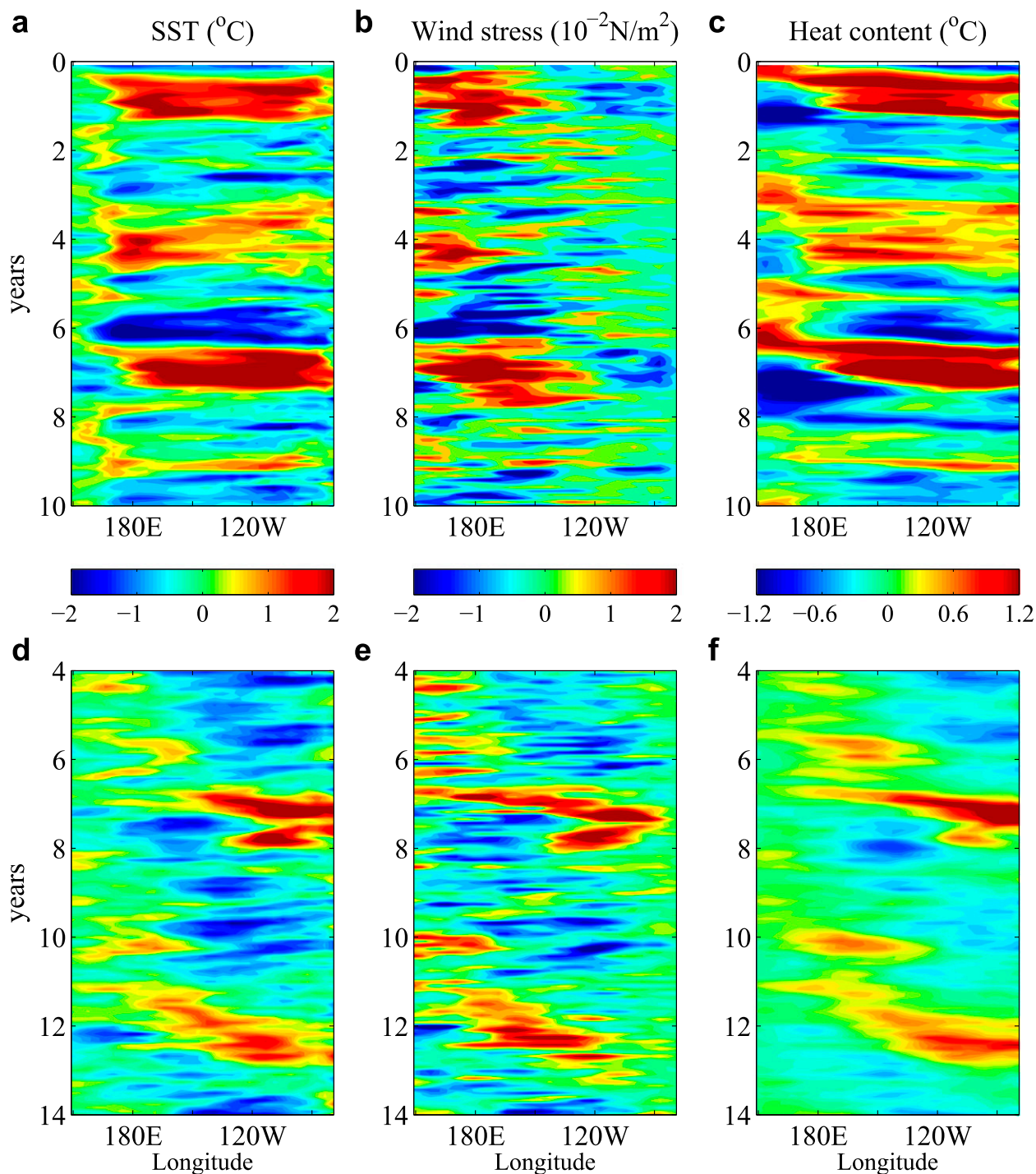


FIG. 7. Hovmöller diagrams for equatorial anomalies of (a),(d) SST, (b),(e) zonal wind stress, and (c),(f) OHC (defined here as temperature averaged between 50 and 300 m) for (a)–(c) the present-day simulation with $\Delta T = 5.6^\circ\text{C}$ and (d)–(f) the simulation with $\Delta T = 1.4^\circ\text{C}$. Note the development of El Niño events and the eastward propagation of ocean heat content anomalies in both climates. Also note a more easterly location of wind stress anomalies at the peak of El Niño events for the small ΔT (cf. Fig. 11). Time on the y axes is consistent with Figs. 4b,d.

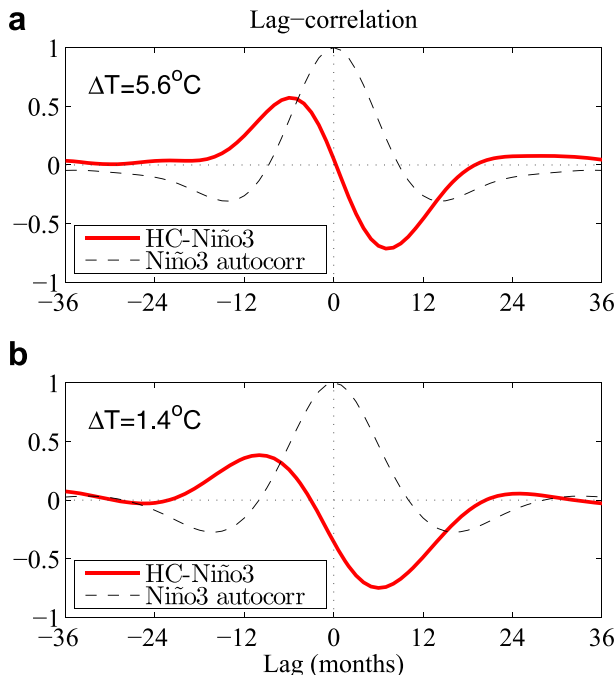


FIG. 8. Lag correlations between OHC anomalies in the western Pacific and the Niño-3 index (solid red lines), and the Niño-3 autocorrelation (dashed black lines), for $\Delta T =$ (a) 5.6°C and (b) 1.4°C . Negative lags indicate that OHC anomalies lead the Niño-3 index. OHC is defined as temperature in the Pacific ocean averaged between 20 and 300 m at 2.5°N – 2.5°S east of 150°W (excluding the Niño-3 region where SST and OHC are highly correlated at zero lag). Note that OHC anomalies lead the Niño-3 index by 6–10 months, indicating the importance of the heat recharge mechanism for ENSO dynamics in both of the experiments.

Negative feedbacks describe the damping of surface temperature anomalies by various processes (Fig. 10b). The main negative feedback involves the damping of SSTs by the mean upwelling of subsurface waters, which decreases for smaller ΔT . The damping of SST by the mean zonal flow also decreases but to a lesser degree. In contrast, the effective thermodynamic damping by surface heat and radiation fluxes increases severalfold. This increase is dominated by the shortwave flux component associated with clouds. As the region of atmospheric convection shifts eastward, anomalies in cloud cover shield the eastern Pacific from shortwave radiation, damping warm SST anomalies. Largely because of this factor, the combined negative feedbacks also strengthen for smaller ΔT .

The total BJ index (the sum of negative and positive feedbacks) remains negative (Fig. 10c), which implies that the model ENSO is controlled by a damped mode across a broad range of climates. Remarkably, despite large variations in negative and positive feedbacks, the magnitude of the BJ index changes relatively little, and the e -folding decay time scale of the ENSO mode in the

model stays close to 1 yr. There is a slight tendency for increased ENSO stability in climates with larger ΔT (Fig. 10c); however, this result should be interpreted with caution in light of the accumulated errors associated with the estimates of different terms constituting the BJ index [see Eq. (3)].

It is worth noting that our estimates of the strength of the linear feedbacks depend to some degree on the chosen size and location of the averaging box and the depth chosen to evaluate subsurface temperature anomalies. For example, we have used the Niño-3 box because it includes the region of maximum SST variance in the cold tongue, but we could have chosen a slightly different region. Nevertheless, having explored the sensitivity of our analysis to these factors, we found that the main conclusions of the study do not change: for smaller ΔT the Ekman feedback overcomes the thermocline feedback, and across all experiments net negative feedbacks exceed positive to give a slightly damped mode with a relatively constant BJ index staying in the range from -1 to -2 yr^{-1} .

We note here that the BJ analysis performed by Kim and Jin (2011), using results from a data assimilation product [Simple Ocean Data Assimilation (SODA); Carton and Giese 2008] and an atmospheric reanalysis [the 40-yr European Centre for Medium-Range Weather Forecasts (ECMWF) Re-Analysis (ERA-40); Simmons and Gibson 2000], shows weaker damping rates, close to 0.25 yr^{-1} . When compared to their study, our climate model overestimates the magnitude of vertical advection and surface thermodynamic damping and underestimates positive effects of thermocline and zonal advection feedbacks. However, the results of Kim and Jin (2011) might easily give an overestimation of the damping rates since the BJ analysis does not take into account the role of atmospheric stochastic processes or other forcing required to sustain a continual oscillation in a damped system. Nor does the BJ analysis consider the effect of nonlinearities important for strong El Niño events. These and other limitations of the BJ analysis, as applied to intercomparison of different climate models, have been recently emphasized by Graham et al. (2014).

c. ENSO period

Across the entire range of simulated climates, the model produces power spectra with a broad interannual peak between 2 and 7 yr clearly distinct from red noise (Fig. 6). The dominant period of ENSO shows a slight increase for smaller ΔT (Fig. 5b), from roughly 3 to 4 yr. This increase in period is related to several factors, including a slowing down of equatorial waves responsible for ocean adjustment. We find that in warmer climates the speed of equatorial Kelvin and Rossby waves

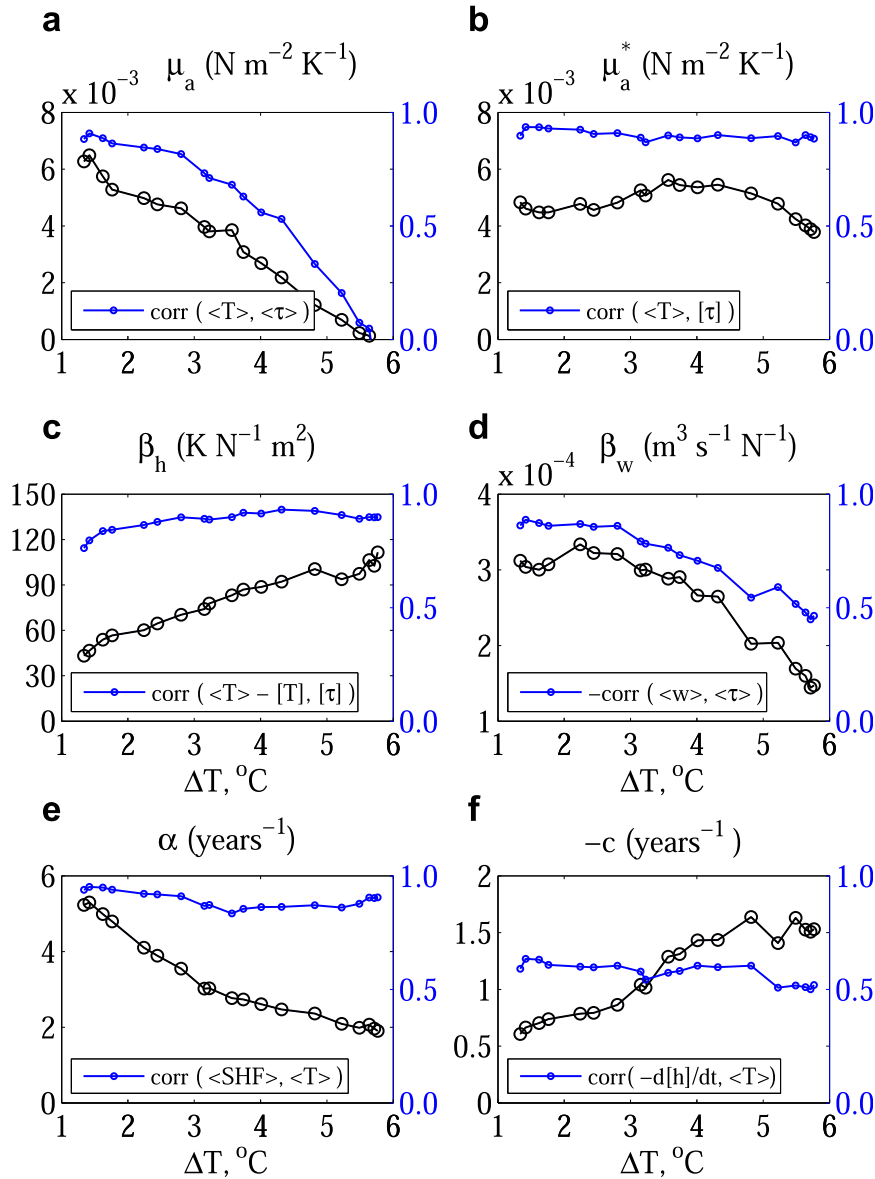


FIG. 9. Most important oceanic and atmospheric sensitivity coefficients (black) as functions of ΔT . Parameters (a) μ_a and (b) μ_a^* showing the sensitivity of Niño-3 and zonally averaged wind stress anomalies to Niño-3 temperature anomalies; (c) β_h showing the sensitivity of the thermocline tilt (defined here as $[h] - \langle h \rangle$) to zonally averaged wind stress; (d) β_w showing the sensitivity of vertical velocity to perturbations in wind stress over the Niño-3 region; (e) α showing the strength of the thermodynamic damping; and (f) parameter c showing the sensitivity of thermocline depth tendency $d[h]/dt$ to Niño-3 temperatures, used in Eq. (2). These sensitivity parameters are obtained by linear regressions between the appropriate time series. The corresponding correlation coefficients are also shown (in blue).

decreases by about 20%–30%, as the weaker ocean stratification overcomes the effect of a deeper thermocline (Fedorov and Philander 2001; Wittenberg 2002; An and Jin 2001). Furthermore, the shift of wind stress anomalies from the western to central Pacific (Fig. 6) lengthens the distance that wind-generated

Rossby waves must travel to reach the basin western boundary. These factors more than compensate the tendency of enhanced Ekman and advection feedbacks to shorten the oscillation period (Yeh et al. 2009; Wittenberg 2002; An and Jin 2001; Fedorov and Philander 2001).

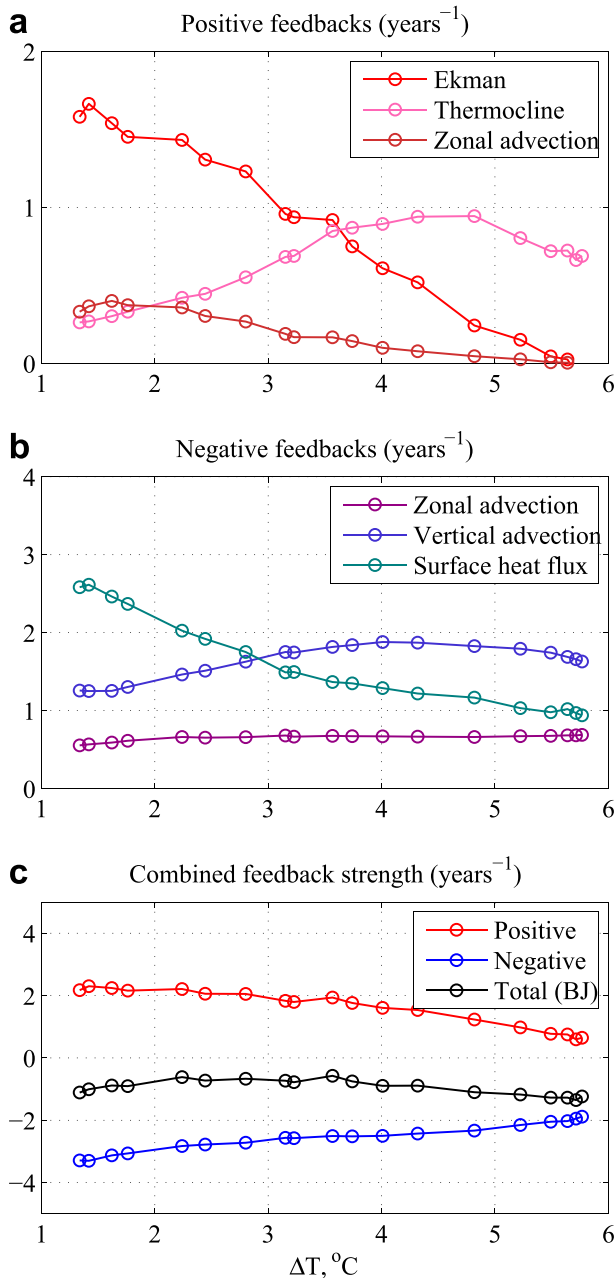


FIG. 10. The strength of ocean-atmosphere feedbacks: (a) positive thermocline, Ekman pumping, and zonal advection feedbacks, (b) negative feedbacks due to the damping of SST anomalies by mean advection and upwelling, and by surface heat fluxes, and (c) net positive and negative feedbacks as well as the total BJ index (black line). The total BJ index is negative, which indicates that the ENSO mode remains damped in all experiments. The magnitude of this index stays fairly constant when ΔT is reduced, mainly because of compensation between the increasing Ekman feedback and the thermodynamic damping.

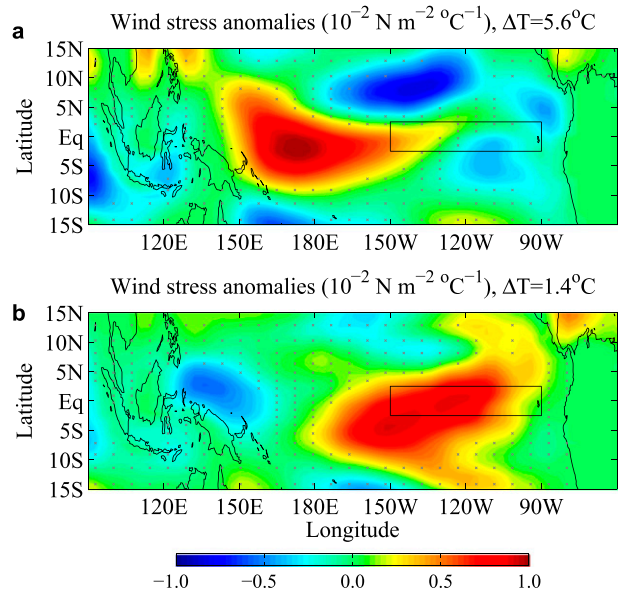


FIG. 11. The typical spatial structure and magnitude of wind stress anomalies in two experiments as given by the regression of wind stress onto the Niño-3 index ($10^{-2} \text{ N m}^{-2} \text{ }^{\circ}\text{C}^{-1}$) for $\Delta T =$ (a) 5.6°C and (b) 1.4°C . For larger values of ΔT , equatorial wind stress anomalies are centered just west of the date line. For smaller ΔT , wind stress anomalies are located closer to the eastern Pacific.

Estimates for the natural oscillation period of ENSO obtained from the damped oscillator model [$2\pi/\Omega_0$, Eqs. (1) and (2)] generally agree with the estimates obtained from the spectral peak of the simulated variability in different experiments (Fig. 12). However, the latter estimates systematically produce longer periods. This is because damping in an oscillatory system driven by noise results in a shift of the spectral peak toward lower frequencies (e.g., Thompson and Battisti 2001).

5. The role of stochastic noise

Our analysis is based on the assumption that the main dynamics of ENSO can be reduced to a low-order dynamical system—the recharge oscillator. However, we have shown that this oscillator is damped (the BJ index is negative; Fig. 10c); therefore, sustaining a continual, albeit irregular, oscillation requires external forcing. Within our framework, this forcing comes from unaccounted physical processes, which can be treated as stochastic noise largely independent of the dominant oscillation. This noise can have atmospheric contributions (e.g., variations in wind stress and surface heat fluxes) as well as oceanic contributions (tropical instability waves, eddies, etc.). Other climate modes, such as the meridional modes (e.g., Zhang et al. 2014), can project on this noise. Furthermore, cumulative action of the neglected nonlinearities can be also considered as part of noise.

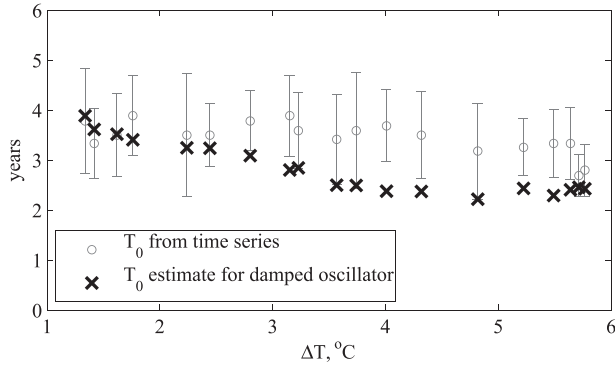


FIG. 12. Estimates for the characteristic ENSO period based on the peak of the power spectra (gray circles with error bars; as in Fig. 5b) and for the natural period of the ENSO mode in the damped oscillator Eq. (5), $2\pi/\Omega_0$ (black crosses). Difference between the two variables is in part due to the effect of damping, which shifts the spectral peak of the simulated ENSO variability toward frequencies lower than Ω_0 .

Some of these processes directly affect Niño-3 temperatures while others affect the ocean thermocline and subsurface temperatures first. For example, the noise originating from surface heat fluxes (because of changes in clouds, or latent and sensible heat fluxes) influences mixed layer temperatures and thus contributes to Niño-3 variance. However, for interannual time scales, it is the generation of thermocline anomalies by uncoupled variations in the equatorial wind stress that appear to be the dominant process in sustaining coupled ocean–atmosphere variability. This stochastic forcing should be added to the second equation of the recharge oscillator model [Eq. (2)].

To estimate the strength of stochastic forcing, let us compute the zonal-mean wind stress anomalies not related to Niño-3 temperatures as $N_\tau = [\tau_x] - \mu_a^*(T)$. This difference, or residual wind stress, gives the uncoupled component of wind stress variations. The decay scale of the autocorrelation function for N_τ is on the order of several months (Fig. 13a), which is much shorter than the characteristic ENSO time scale, and thus N_τ can be treated as noise. When the system moves toward smaller values of ΔT , its magnitude (standard deviation) decreases by about 30% (Fig. 13b), which is associated with the weakening of the Walker circulation. The simulated decrease of Niño-3 variance in climates with small ΔT (Fig. 5a) is consistent with such a change in the stochastic forcing.

6. Summary and discussion

We have presented a sensitivity analysis of ENSO dependence on the background state of the Pacific Ocean characterized by different mean east–west SST

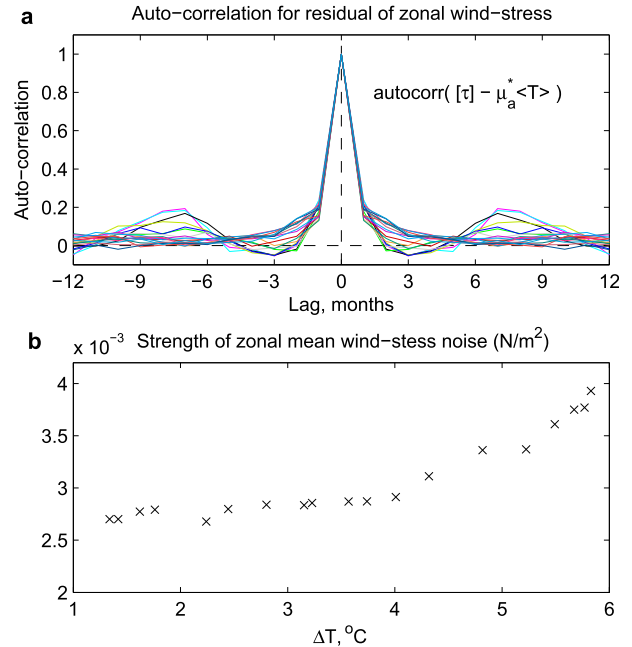


FIG. 13. (a) Autocorrelation function for the residual zonal-mean wind stress anomalies, $N_\tau = [\tau_x] - \mu_a^*(T)$; by definition these residual wind stress anomalies are uncorrelated with Niño-3 temperature anomalies. Each line corresponds to a different climate. The weak secondary maxima of the autocorrelation function are related to the semiannual cycle in zonal wind stress. (b) Characteristic magnitude of the wind stress noise, defined as the standard deviation of N_τ , as a function of ΔT .

gradients within a state-of-the-art climate model. In effect, this study revisits some of the results of Fedorov and Philander (2000, 2001) but using a comprehensive coupled model.

To alter tropical climate, we apply an idealized approach in which we vary ocean vertical diffusivity in the extratropics. By controlling the temperature of water subducted in the STCs, changes in the extratropical mixing indirectly but efficiently modify the tropical Pacific climatology. With the imposed reduction of the mean east–west gradient SST gradient, we observe the weakening of the Walker circulation and the eastward expansion of the convection region in the atmosphere, the deepening of the tropical thermocline, and the weakening of vertical stratification in the ocean.

We find that the simulated ENSO remains robust through broad changes in the east–west SST gradient—from 6° to nearly 1°C (accompanied by significant changes in mean zonal winds and thermocline depth). With these changes, the ENSO amplitude reduces from approximately 1° to $0.6^\circ\text{--}0.7^\circ\text{C}$, and the dominant period lengthens albeit slightly. As we show, across all of these experiments ENSO dynamics are described by the recharge-oscillator framework, which allows us to conduct

a stability analysis based on the BJ index. The BJ analysis shows only modest changes in the period and damping rates of the ENSO mode, consistent with the relatively small changes in the simulated ENSO.

Within the stability analysis we investigate how the imposed changes in the coupled ocean–atmosphere system alter the strengths of the key coupled feedbacks associated with ENSO. In experiments with small ΔT the thermocline feedback is weakened whereas the Ekman feedback dominates among the different positive feedbacks—a situation opposite to the present-day climate. The increase in Ekman feedback is associated with the dramatic eastward shift of the wind stress anomalies. The strengthening of this positive feedback is largely compensated by the increase in thermodynamic damping (mainly because of a stronger shortwave damping of Niño-3 anomalies by cloud feedbacks). As a result, the ENSO mode remains damped throughout the experiments and its damping time scales stay close to about 1 yr.

Current projections for the mean state changes in the tropical Pacific with global warming included a slight weakening of the east–west SST gradient, on the order of 0.5°C (DiNezio et al. 2009). This brings about the question of the extent that our results may be relevant to the problem of potential changes in ENSO with future climate change. We should emphasize, however, that the projected changes in oceanic stratification in the tropical Pacific are different from our experiments. Namely, global warming simulations produce a sharper and shallower ocean thermocline along the equator (Vecchi and Soden 2007), which may limit the applicability of our results to the global warming problem.

Nevertheless, the compensation between positive and negative feedbacks in our study seems to mirror the compensation between different feedbacks predicted to occur under global warming (Collins et al. 2010; DiNezio et al. 2012). In our experiments, the counterbalance (or compensation) between different feedbacks is related to the induced changes in the Walker circulation. For smaller values of ΔT , atmospheric convection spreads eastward and so do wind stress anomalies, strengthening the Ekman feedback. At the same time, because of the moistening of the lower troposphere in the eastern Pacific, cloud cover anomalies over the Niño-3 region also amplify, leading to a stronger damping. Thus, the increased damping and increased Ekman feedback have the same origin and occur side by side. Similarly, compensation between different feedbacks can occur under global warming scenarios. In particular, DiNezio et al. (2012) argued that in doubling-of- CO_2 simulations, a reduction in the thermocline feedback due to the weakening of the mean Walker cell is compensated by a strengthening of the

advection feedback due to a greater subsurface temperature contrast, also related to the weakening of the Walker cell, albeit indirectly.

Finally, we should also point to several other limitations of the present study. For example, we do not address the ultimate causes of changes in the zonal SST gradient—we simply induce those changes from the extratropics. Consequently, we do not explicitly consider changes in tropical climate caused by variations in Earth's precession or obliquity (Clement et al. 1999; Timmermann et al. 2007; Clement et al. 2000), volcanic or solar forcing (Mann et al. 2005), or high CO_2 levels (Cherchi et al. 2008). A significant reduction of the mean east–west SST gradient can also be achieved by other means, such as by varying cloud properties within a climate model (Burls and Fedorov 2014). Nevertheless, although some of our results might be model or approach dependent, the major physical inferences should hold (e.g., the eastward shift of wind anomalies or feedback compensation for smaller ΔT).

Despite the limitations, our results have important implications, especially for paleoclimates. In particular, the robustness of ENSO through a wide range of simulated climate agrees with the available observational evidence of ENSO in different geological epochs (Fig. 1). Contrary to suggestions in Davies et al. (2012, 2011) and Watanabe et al. (2011), a weak mean zonal SST gradient (“permanent El Niño-like” conditions) and active ENSO do not preclude one another. For small values of ΔT , one could expect a reduction of ENSO magnitude but not its full disappearance.

Finally, we should emphasize that we do not claim in this study that there are no changes in the properties of ENSO across the different climates we considered. In fact, we observe dramatic changes in the relative importance of the key feedbacks, changes in the typical amplitude and periodicity of the events, and changes in the propagation characteristics of SST anomalies, among others. However, given the strong imposed modification in the background tropical climate, the ENSO amplitudes changes relatively little and the overall ENSO dynamics remain very robust.

Acknowledgments. Financial support was provided by the grants from the U.S. Department of Energy Office of Science (DE-SC0007037), NSF (AGS-1405272), and the David and Lucile Packard Foundation. Support from the Yale University Faculty of Arts and Sciences High Performance Computing facility is acknowledged. We thank Chris Brierley, Natalie Burls, Christina Ravelo, and George Philander for discussions of this topic and the anonymous reviewers for help in clarifying key issues in the paper.

REFERENCES

- An, S.-I., and F.-F. Jin, 2000: An eigen analysis of the interdecadal changes in the structure and frequency of ENSO mode. *Geophys. Res. Lett.*, **27**, 2573–2576, doi:10.1029/1999GL011090.
- , and —, 2001: Collective role of thermocline and zonal advective feedbacks in the ENSO mode. *J. Climate*, **14**, 3421–3432, doi:10.1175/1520-0442(2001)014<3421:CROTAZ>2.0.CO;2.
- Bellenger, H., E. Guilyardi, J. Leloup, M. Lengaigne, and J. Vialard, 2013: ENSO representation in climate models: From CMIP3 to CMIP5. *Climate Dyn.*, **42**, 1999–2018, doi:10.1007/s00382-013-1783-z.
- Brown, J., M. Collins, and A. Tudhope, 2006: Coupled model simulations of mid-Holocene ENSO and comparisons with coral oxygen isotope records. *Adv. Geosci.*, **6**, 29–33, doi:10.5194/adgeo-6-29-2006.
- Brown, J. N., A. V. Fedorov, and E. Guilyardi, 2011: How well do coupled models replicate ocean energetics relevant to ENSO? *Climate Dyn.*, **36**, 2147–2158, doi:10.1007/s00382-010-0926-8.
- Burls, N. J., and A. V. Fedorov, 2014: What controls the mean east-west sea surface temperature gradient in the equatorial Pacific: The role of cloud albedo. *J. Climate*, **27**, 2757–2778, doi:10.1175/JCLI-D-13-00255.1.
- Cane, M. A., 2005: The evolution of El Niño, past and future. *Earth Planet. Sci. Lett.*, **230**, 227–240.
- Carton, J. A., and B. S. Giese, 2008: A reanalysis of ocean climate using Simple Ocean Data Assimilation (SODA). *Mon. Wea. Rev.*, **136**, 2999–3017, doi:10.1175/2007MWR1978.1.
- Cherchi, A., S. Masina, and A. Navarra, 2008: Impact of extreme CO₂ levels on tropical climate: A CGCM study. *Climate Dyn.*, **31**, 743–758, doi:10.1007/s00382-008-0414-6.
- Clarke, A. J., 2008: *An Introduction to the Dynamics of El Niño and the Southern Oscillation*. Elsevier, 324 pp.
- Clement, A. C., R. Seager, and M. A. Cane, 1999: Orbital controls on the El Niño/Southern Oscillation and the tropical climate. *Paleoceanography*, **14**, 441–456, doi:10.1029/1999PA900013.
- , —, and —, 2000: Suppression of El Niño during the mid-Holocene by changes in the Earth's orbit. *Paleoceanography*, **15**, 731–737, doi:10.1029/1999PA000466.
- Cobb, K. M., C. D. Charles, H. Cheng, and R. L. Edwards, 2003: El Niño/Southern Oscillation and tropical Pacific climate during the last millennium. *Nature*, **424**, 271–276, doi:10.1038/nature01779.
- , N. Westphal, H. R. Sayani, J. T. Watson, E. Di Lorenzo, H. Cheng, R. Edwards, and C. D. Charles, 2013: Highly variable El Niño–Southern Oscillation throughout the Holocene. *Science*, **339**, 67–70, doi:10.1126/science.1228246.
- Collins, M., and Coauthors, 2010: The impact of global warming on the tropical Pacific Ocean and El Niño. *Nat. Geosci.*, **3**, 391–397, doi:10.1038/ngeo868.
- Davies, A., A. E. Kemp, and H. Pälike, 2011: Tropical ocean–atmosphere controls on inter-annual climate variability in the Cretaceous Arctic. *Geophys. Res. Lett.*, **38**, L03706, doi:10.1029/2010GL046151.
- , —, G. P. Weedon, and J. A. Barron, 2012: El Niño–Southern Oscillation variability from the late Cretaceous Marcellus shale of California. *Geology*, **40**, 15–18, doi:10.1130/G32329.1.
- Dekens, P. S., A. C. Ravelo, M. D. McCarthy, and C. A. Edwards, 2008: A 5 million year comparison of Mg/Ca and alkenone paleothermometers. *Geochem. Geophys. Geosyst.*, **9**, Q10001, doi:10.1029/2007GC001931.
- DiNezio, P. N., A. C. Clement, G. A. Vecchi, B. J. Soden, B. P. Kirtman, and S.-K. Lee, 2009: Climate response of the equatorial Pacific to global warming. *J. Climate*, **22**, 4873–4892, doi:10.1175/2009JCLI2982.1.
- , B. P. Kirtman, A. C. Clement, S.-K. Lee, G. A. Vecchi, and A. Wittenberg, 2012: Mean climate controls on the simulated response of ENSO to increasing greenhouse gases. *J. Climate*, **25**, 7399–7420, doi:10.1175/JCLI-D-11-00494.1.
- Fedorov, A. V., 2010: Ocean response to wind variations, warm water volume, and simple models of ENSO in the low-frequency approximation. *J. Climate*, **23**, 3855–3873, doi:10.1175/2010JCLI3044.1.
- , and S. G. Philander, 2000: Is El Niño changing? *Science*, **288**, 1997–2002, doi:10.1126/science.288.5473.1997.
- , and —, 2001: A stability analysis of tropical ocean–atmosphere interactions: Bridging measurements and theory for El Niño. *J. Climate*, **14**, 3086–3101, doi:10.1175/1520-0442(2001)014<3086:ASAOTO>2.0.CO;2.
- , P. Dekens, M. McCarthy, A. Ravelo, P. DeMenocal, M. Barreiro, R. Pacanowski, and S. Philander, 2006: The Pliocene paradox (mechanisms for a permanent El Niño). *Science*, **312**, 1485–1489, doi:10.1126/science.1122666.
- , C. Brierley, and K. Emanuel, 2010: Tropical cyclones and permanent El Niño in the early Pliocene epoch. *Nature*, **463**, 1066–1070, doi:10.1038/nature08831.
- , —, K. Lawrence, Z. Liu, P. Dekens, and A. Ravelo, 2013: Patterns and mechanisms of early Pliocene warmth. *Nature*, **496**, 43–49, doi:10.1038/nature12003.
- Ford, H. L., A. C. Ravelo, and S. Hovan, 2012: A deep eastern equatorial Pacific thermocline during the early Pliocene warm period. *Earth Planet. Sci. Lett.*, **355**, 152–161, doi:10.1016/j.epsl.2012.08.027.
- Galeotti, S., A. von der Heydt, M. Huber, D. Bice, H. Dijkstra, T. Jilbert, L. Lanci, and G.-J. Reichert, 2010: Evidence for active El Niño Southern Oscillation variability in the late Miocene greenhouse climate. *Geology*, **38**, 419–422, doi:10.1130/G30629.1.
- Graham, F. S., and Coauthors, 2014: Effectiveness of the Bjerknes stability index in representing ocean dynamics. *Climate Dyn.*, doi:10.1007/s00382-014-2062-3, in press.
- Gu, D., and S. G. Philander, 1997: Interdecadal climate fluctuations that depend on exchanges between the tropics and extratropics. *Science*, **275**, 805–807, doi:10.1126/science.275.5301.805.
- Guilyardi, E., A. Wittenberg, A. Fedorov, M. Collins, C. Wang, A. Capotondi, G. J. van Oldenborgh, and T. Stockdale, 2009: Understanding El Niño in ocean–atmosphere general circulation models: Progress and challenges. *Bull. Amer. Meteor. Soc.*, **90**, 325–340, doi:10.1175/2008BAMS2387.1.
- Huber, M., and R. Caballero, 2003: Eocene El Niño: Evidence for robust tropical dynamics in the “hothouse.” *Science*, **299**, 877–881, doi:10.1126/science.1078766.
- Ivany, L. C., T. Brey, M. Huber, D. P. Buick, and B. R. Schöne, 2011: El Niño in the Eocene greenhouse recorded by fossil bivalves and wood from Antarctica. *Geophys. Res. Lett.*, **38**, L16709, doi:10.1029/2011GL048635.
- Jin, F.-F., 1997a: An equatorial ocean recharge paradigm for ENSO. Part I: Conceptual model. *J. Atmos. Sci.*, **54**, 811–829, doi:10.1175/1520-0469(1997)054<0811:AEORPF>2.0.CO;2.
- , 1997b: An equatorial ocean recharge paradigm for ENSO. Part II: Conceptual model. *J. Atmos. Sci.*, **54**, 830–847, doi:10.1175/1520-0469(1997)054<0830:AEORPF>2.0.CO;2.
- , S. T. Kim, and L. Bejarano, 2006: A coupled-stability index for ENSO. *Geophys. Res. Lett.*, **33**, L23708, doi:10.1029/2006GL027221.

- Kim, S. T., and F.-F. Jin, 2011: An ENSO stability analysis. Part II: Results from the twentieth and twenty-first century simulations of the CMIP3 models. *Climate Dyn.*, **36**, 1609–1627, doi:10.1007/s00382-010-0872-5.
- Koutavas, A., P. B. deMenocal, G. C. Olive, and J. Lynch-Stieglitz, 2006: Mid-Holocene El Niño–Southern Oscillation (ENSO) attenuation revealed by individual foraminifera in eastern tropical Pacific sediments. *Geology*, **34**, 993–996, doi:10.1130/G22810A.1.
- Mann, M. E., M. A. Cane, S. E. Zebiak, and A. Clement, 2005: Volcanic and solar forcing of the tropical Pacific over the past 1000 years. *J. Climate*, **18**, 447–456, doi:10.1175/JCLI-3276.1.
- Manucharyan, G., C. Brierley, and A. Fedorov, 2011: Climate impacts of intermittent upper ocean mixing induced by tropical cyclones. *J. Geophys. Res.*, **116**, C11038, doi:10.1029/2011JC007295.
- McCreary, J. P., Jr., and P. Lu, 1994: Interaction between the subtropical and equatorial ocean circulations: The subtropical cell. *J. Phys. Oceanogr.*, **24**, 466–497.
- McGregor, S., A. Timmermann, M. H. England, O. Elison Timm, and A. T. Wittenberg, 2013: Inferred changes in El Niño–Southern Oscillation variance over the past six centuries. *Climate Past*, **9**, 2269–2284, doi:10.5194/cp-9-2269-2013.
- Meinen, C. S., and M. J. McPhaden, 2000: Observations of warm water volume changes in the equatorial Pacific and their relationship to El Niño and La Niña. *J. Climate*, **13**, 3551–3559, doi:10.1175/1520-0442(2000)013<3551:OOWWVC>2.0.CO;2.
- Philander, S. G., 1990: *El Niño, La Niña, and the Southern Oscillation*. Academic Press, 293 pp.
- Ravelo, A. C., 2008: Lessons from the Pliocene Warm Period and the onset of Northern Hemisphere glaciation. *2008 Fall Meeting*, San Francisco, CA, Amer. Geophys. Union, Abstract PP23E-01.
- Rittenour, T. M., J. Brigham-Grette, and M. E. Mann, 2000: El Niño-like climate teleconnections in New England during the late Pleistocene. *Science*, **288**, 1039–1042, doi:10.1126/science.288.5468.1039.
- Sarachik, E. S., and M. A. Cane, 2010: *The El Niño–Southern Oscillation Phenomenon*. Cambridge University Press, 369 pp.
- Scroton, N., S. Bonham, R. Rickaby, S. Lawrence, M. Hermoso, and A. Haywood, 2011: Persistent El Niño–Southern Oscillation variation during the Pliocene epoch. *Paleoceanography*, **26**, PA2215, doi:10.1029/2010PA002097.
- Shields, C. A., D. A. Bailey, G. Danabasoglu, M. Jochum, J. T. Kiehl, S. Levis, and S. Park, 2012: The low-resolution CCSM4. *J. Climate*, **25**, 3993–4014, doi:10.1175/JCLI-D-11-00260.1.
- Simmons, A. J., and J. Gibson, 2000: The ERA-40 project plan. ECMWF. [Available online at <http://old.ecmwf.int/research/era/Project/Plan/index.html>.]
- Sun, D.-Z., 2003: A possible effect of an increase in the warm-pool SST on the magnitude of El Niño warming. *J. Climate*, **16**, 185–205, doi:10.1175/1520-0442(2003)016<0185:APEOAI>2.0.CO;2.
- , T. Zhang, and S.-I. Shin, 2004: The effect of subtropical cooling on the amplitude of ENSO: A numerical study. *J. Climate*, **17**, 3786–3798, doi:10.1175/1520-0442(2004)017<3786:TEOSCO>2.0.CO;2.
- Thompson, C., and D. Battisti, 2001: A linear stochastic dynamical model of ENSO. Part II: Analysis. *J. Climate*, **14**, 445–466, doi:10.1175/1520-0442(2001)014<0445:ALSDMO>2.0.CO;2.
- Timmermann, A., S. Lorenz, S. An, A. Clement, and S. Xie, 2007: The effect of orbital forcing on the mean climate and variability of the tropical Pacific. *J. Climate*, **20**, 4147–4159, doi:10.1175/JCLI4240.1.
- Vecchi, G. A., and B. J. Soden, 2007: Global warming and the weakening of the tropical circulation. *J. Climate*, **20**, 4316–4340, doi:10.1175/JCLI4258.1.
- Wara, M. W., A. C. Ravelo, and M. L. Delaney, 2005: Permanent El Niño-like conditions during the Pliocene warm period. *Science*, **309**, 758–761, doi:10.1126/science.1112596.
- Watanabe, M., J.-S. Kug, F.-F. Jin, M. Collins, M. Ohba, and A. T. Wittenberg, 2012: Uncertainty in the ENSO amplitude change from the past to the future. *Geophys. Res. Lett.*, **39**, L20703, doi:10.1029/2012GL053305.
- Watanabe, T., and Coauthors, 2011: Permanent El Niño during the Pliocene warm period not supported by coral evidence. *Nature*, **471**, 209–211, doi:10.1038/nature09777.
- Wittenberg, A. T., 2002: ENSO response to altered climates. Ph.D. thesis, Princeton University, 475 pp.
- , 2004: Extended wind stress analyses for ENSO. *J. Climate*, **17**, 2526–2540, doi:10.1175/1520-0442(2004)017<2526:EWSAFE>2.0.CO;2.
- Yeh, S.-W., J.-S. Kug, B. Dewitte, M.-H. Kwon, B. P. Kirtman, and F.-F. Jin, 2009: El Niño in a changing climate. *Nature*, **461**, 511–514, doi:10.1038/nature08316.
- Zhang, H., A. Clement, and P. Di Nezio, 2014: The South Pacific meridional mode: A mechanism for ENSO-like variability. *J. Climate*, **27**, 769–783, doi:10.1175/JCLI-D-13-00082.1.